Comparative analysis of time-like hyperon form factors

Andrea Bianconi[*]

Dipartimento di Ingegneria dell'Informazione, Università degli Studi di Brescia and Istituto Nazionale di Fisica Nucleare,
Gruppo Collegato di Brescia, I-25133 Brescia, Italy

Egle Tomasi-Gustafsson [ORCID][†]

DPhN, IRFU, CEA, Université Paris-Saclay, 91191 Gif-sur-Yvette Cedex, France

Data on hyperon form factors recently obtained from annihilation reactions are compared to each other and to proton and neutron form factors, in terms of two kinematical variables: the transferred momentum square, q^2, and the modulus P of the relative momentum between the outgoing baryons. They are critically discussed in terms of possible correlated structures. The present status of the time-like form factor data for baryons is described and suggestions are given on the reactions and the kinematical range where data are desirable in order to clarify the arisen questions.

I. INTRODUCTION

A. General background

The internal properties of composite particles are conveniently expressed in terms of form factors (FFs) (for a review see Refs. [1,2]). FFs are measured in elastic $eh \rightarrow eh$ scattering and in annihilation reactions as $e^+e^- \leftrightarrow h\bar{h}$, where h is a hadron. Form factors are Lorentz scalar functions of the only one variable q^2, q being the four-momentum of the virtual photon, which mediates in the t and s channel, respectively, the scattering and the annihilation processes in the Born approximation. The scattering reaction covers the region of space-like momenta, $q^2 < 0$, whereas the annihilation reactions give information on the time-like region of transferred momenta, $q^2 > 0$.

This work focuses on FFs data in the time-like region, from electron positron colliders. Although data on the proton and neutron time-like electromagnetic FFs (TLFF) have a long history, the precision of recent experiments has recently opened a debate on aspects of the TLFF that cannot be simply deduced or guessed by extrapolating space-like properties.

Since the FENICE experiment at Frascati in 1994 [3], new precise measurements from modern colliders added precious information in the time-like region, particularly on neutrons

and hyperons. The high luminosity obtained at the present e^+e^- colliders opens the opportunity to apply the quasireal electron method [4], also called initial state radiation (ISR) technique, to experiments such as BABAR and BESIII. It allows us to extract e^+e^--annihilated cross section values from the differential cross section data of processes where a real hard photon is emitted from one of the lepton beams and is detected, allowing the selection of the four-momentum transferred to the final hadron pair, as for a beam energy-scan. The large center-of-mass energy of modern colliders brings the advantage to obtain, by means of the ISR technique, data in a wide region of q^2 and with a high level of accuracy, despite the reduction of the cross section by a factor of $\alpha_{EM} \simeq 1/137$, the fine structure constant, which is indeed compensated by the high luminosity.

BABAR gave the first very precise measurements on proton FF in a wide region, up to 40 points for $4.25 \leqslant q^2 \leqslant 36$ GeV^2 [5,6]. These data show evidence of specific structures, which become regular when plotted as a function of P, the modulus of relative three-momentum of the proton-antiproton pair in the final state, as discovered in a series of articles [7–9]. Repeating the same analysis, these oscillations were confirmed on the proton by BESIII both with the ISR method [10,11] and with the energy scan method [12], and more recently on the neutron FF data, described by oscillations differing from the proton ones by a phase [13].

Hyperon TLFFs were also measured, although with less precision with respect to the nucleon FFs. The BESIII experiment [14] measured the $e^+e^- \rightarrow \Lambda\bar{\Lambda}$ cross section at four energies, namely: $\sqrt{s} = 2.2324$, 2.400, 2.800 and 3.080 GeV, lying in the same range already investigated by the BABAR experiment, but with better precision. Recently, high-energy cross section measurements were given in Ref. [15] with the aim to find evidence of the $\psi(3770)$ vector meson. The BESIII experiment [16] measured at six energy points the $\Sigma^+\bar{\Sigma}^-$ and

at three points the $\Sigma^-\bar{\Sigma}^+$ cross sections [16,17] by extracting the corresponding TLFFs, while the BABAR experiment measured the $\Sigma^0\bar{\Sigma}^0$ as well as the $\Lambda\bar{\Sigma}^0$ + c.c. cross sections, giving their TLFFs and transition TLFFs [18], respectively. The CLEO experiment [19] also measured cross sections and extracted TLFFs of several hyperons in the kinematical region around the mass of the $\psi(3770)$ vector meson. These data will not be used in the present analysis, as they are less precise than the most recent ones.

The BESIII experiment has also obtained values of the TLFFs of the Ξ hyperons, namely: eight values for the charged Ξ^- [20] and ten for the neutral Ξ^0 [21], all of them belonging to the energy interval [2.644, 3.080] GeV. Note that, although the baryons Σ^+, Σ^0, and Σ^- form an isospin triplet, the Σ^- is not the antiparticle of the Σ^+, so there are two different TLFFs corresponding to the final state $\Sigma^+\bar{\Sigma}^-$ and $\Sigma^-\bar{\Sigma}^+$.

All through the paper, natural units are used, so that $\hbar = c = 1$.

B. Irregularities in the proton tlffs

Thanks to the high luminosity available at the colliders, only recently experiments could collect enough statistics to make possible the extraction of the individual moduli of the electric and magnetic TLFFs. However, from the cross section of the annihilation $e^+e^- \rightarrow h\bar{h}$, where h is a spin-1/2 hadron, in the Born approximation one can always define the effective TLFF F_h as

$$F_h^2(q^2) \equiv A_E(q^2)|G_E(q^2)|^2 + A_M(q^2)|G_M(q^2)|^2, \quad (1)$$

where A_E and A_M are kinematic coefficients, q is the four-momentum of the $h\bar{h}$ system, and hence q^2 is the squared value of the center-of-mass energy. The total cross section in this frame can be written as:

$$\sigma(q^2) = K(q^2)F_h^2(q^2), \quad (2)$$

where $K(q^2)$ is a known kinematic factor. An interesting aspect is the presence of small oscillations in the proton effective TLFF, the systematic character of which has been highlighted in Ref. [7], after decomposing F_p as a sum of two terms: a regular background and an oscillation term, namely

$$F_p(q^2) \equiv F_{\text{bkg}}(q^2) + F_{\text{osc}}(P), \quad (3)$$

where P is the modulus of the relative three-momentum of the final $p\bar{p}$ pair (see later for the definition).

The background term describes a regular decrease not far from the known $(1/q^2)^2$ quark counting rule [22,23] while the modulation term has the form

$$F_{\text{osc}}(P) = A\, e^{-BP}\cos(CP + D), \quad (4)$$

with A, B, C, and D to be determined accordingly to the data. At the condition of a moderate exponential decrease, this describes quasiperiodic oscillations. Several background terms taken from the literature have been tested in Ref. [7], as a standard dipole, and the conclusions did not depend on the choice. In all cases the fitted values of A and B imply that the oscillation amplitude is about 5–10 % of the background in all the relevant range, C corresponds to the oscillation

period $2\pi/C \simeq 1.1$ GeV, and $D \approx 0$ indicates that there is an oscillation maximum at the $p\bar{p}$ production threshold, where $P = 0$.

Irregularities in a few-GeV hadronic state are not a surprise, but their periodicity opened a question on the underlying mechanism. The modulation may be interpreted as a self-coherent pattern (possibly of interference origin), but it may be a set of three independent resonances, as suggested in Ref. [24]. These two interpretations are not necessarily antagonistic, if the formation of a group of resonances is due to some simple and common underlying mechanism. For example a toy model on the pion TLFF predicts a periodic sequence of resonances [25].

By making Fourier transforms, the analysis carried out in Ref. [7] associates the oscillation period to a space-time dimension of 1 fm, implying a nonscaling mechanism acting on such a scale. As a consequence, one expects the oscillations to disappear when q^2 becomes large enough to reach the expected $\simeq (1/q^2)^2$ asymptotic behavior.

A more theoretical analysis was carried out in Refs. [8,9], showing that energy-periodic oscillations are present when two almost identical, but slightly shifted in time, formation pathways compete to reach the same final state. Since the increasing space distance r between the baryon and the antibaryon in the final state is, in the average, proportional to the time, an interference in time corresponds to an interference in space and, hence, in the distance r. The hadron-antihadron relative three-momentum $\vec{P}$ is the conjugate variable of the distance $\vec{r}$.

On the other side, the most recent BESIII data on proton TLFF have included several values of the ratio $|R| = |G_E/G_M|$. Complemented by BABAR [5,6] and Novosibirsk [26] data on F_p that span a region down to threshold, where the constraint $G_E(4M_p^2) = G_M(4M_p^2)$, holds (being M_p the proton mass), a continuous description of $|G_E|$ and $|G_M|$ in a wide range of q^2 was given in the form of a physics driven fit [27]. $|G_E|$ and $|G_M|$ do not appear to be periodic functions of P, in contrast with their combination F_p. Whether the periodicity of F_p is there by mere chance or not is still to be clarified. This leads to a more general question, that is, whether F_p may have a meaning as an effective amplitude, or must just be considered as the real and positive squared root of a linear combination of $|G_E|^2$ and $|G_M|^2$ from Eq. (1).

C. Proton and neutron time-like form factors

An analysis of pre-BESIII data had shown the presence of near-threshold enhancements in neutron and neutral baryon TLFFs [28]. Later, BESIII data [13] on the neutron TLFF have shown oscillations as well. Adopting the technique of Ref. [7], the authors of this measurement have interpolated the neutron FF data according to Eqs. (3), (4), finding best-fit results with the same period of the proton data (in the variable P) and a 120° phase shift. Two weak points of these results are (i) some gaps in the data range leave ambiguity on the precise shape of the neutron curve, (ii) by comparing the proton data fit of Ref. [13] with those of Refs. [8,27], one finds that the phase of the proton oscillating component depends on the choice of the background component when the expression of

Eq. (3) is used. The oscillation period is, however, reasonably background independent.

A confirmation of this correlation by a more complete set of data would support the presence of relevant channel mixing in the production mechanisms of $\gamma^* \to p\bar{p}$ and $\gamma^* \to n\bar{n}$. An analysis of the constraint posed by the present data on this mixing has been carried out in Ref. [29] under the assumption that the isoscalar, $I = 0$, and isovector, $I = 1$, states are independently formed in the electromagnetic initial part of the process and not later remixed. Although the confirmation of a channel mixing would be a relevant phenomenon in itself, expressing $p\bar{p}$ and $n\bar{n}$ in terms of other states does not explain the origin of the $p\bar{p}$ and $n\bar{n}$ irregularities. This means that either the isospin channels do independently oscillate, or alternatively that they have an energy-dependent relative phase $\phi(q^2)$. In any case, the origin of the oscillations or of $\phi(q^2)$ remains unknown.

Summarizing the state of the art with irregularities in the nucleon TLFFs, it is evident that peculiar time-like phenomena are present. It is not clear whether they derive from processes that may be similar, but independently affect the $p\bar{p}$ and $n\bar{n}$ channels, or are connected to some degree of channel mixing. It is also not clear whether we are seeing an overlap of independent processes (such as three resonances) or the effects of a unique underlying mechanism (such as two interfering amplitudes, or flux exchange between $p\bar{p}$ and $n\bar{n}$ final states).

Very recently, a joint analysis of SL and TL proton and neutron data based on dispersion relations has been carried out in Ref. [30]. This allows for a complete model of the moduli and phases of G_E and G_M for both nucleons.

D. Baryon form factors and aims of the present work

In addition to nucleon TLFFs, several sets of data have been collected on strange hyperon effective TLFFs. These data, at first sight, support the possibility of additional non-monotonous and irregular behaviors. However, at present, their precision and distribution do not allow us to shed light on the dynamical mechanisms underlying such behaviors. It is quite difficult to reproduce these data in an unambiguous way, as evident in some of the proposed fits of Ref. [31]. Apart from fitting difficulties, the question is what we may understand from these data on the underlying processes.

The aim of the present work is to organize the hyperon data and find correlations or common behaviors among them and with the nucleon TLFFs, to gain further insight on the discussed problems. Waiting for more precision and statistics in the measurements of the years to come, we feel that it is better not to stick to very specific models such as the oscillations of Eq. (4). We will rather try to identify correlations and common trends in the available data on proton, neutron, and several strange baryon TLFF, including data on the $\Lambda\bar{\Sigma}^0$ transition TLFF, which parametrize the effective amplitude of the process $\gamma^* \to \Lambda\bar{\Sigma}^0 +$ c.c..

The cases of the neutron and the proton, as well as their comparison, have been already discussed in Refs. [13,31]. A dedicated analysis will be published in a forthcoming paper. We will only marginally discuss the relations between the
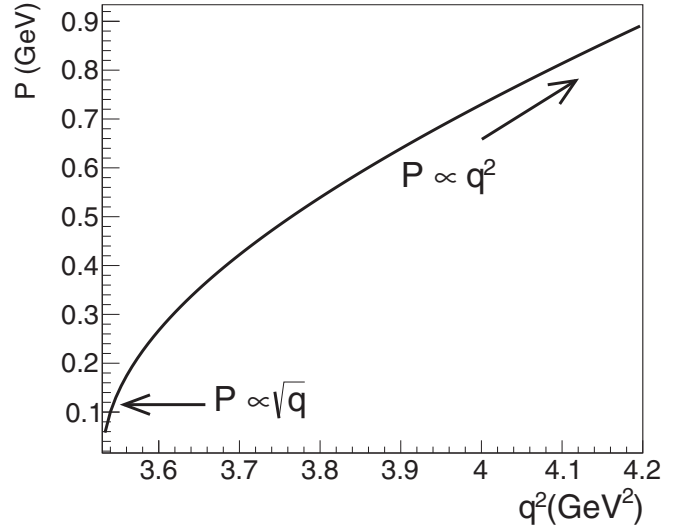

FIG. 1. Relation between P and q^2 from Eq. (5), for the $n\bar{n}$ channel. The red arrows and the formulas highlight the high-q^2 and the near-threshold limits, given by Eq. (6).

proton and neutron TLFFs, although we will frequently compare hyperon and nucleon data.

We do not make fits, however, when it will be the case, straight lines will be used to highlight particular behaviors, mainly to avoid too crowded graphs,. For instance, in semilog plots in the P variable, straight lines would correspond to exponential trends of the kind e^{-aP}, a is a constant. If one plots in the same graph all the available data on baryon TLFFS as a function of q^2 or P, the graph would be poorly readable. Thus, we will present only small samples of data within selected ranges, e.g., the near-threshold and the preasymptotic regions.

II. METHOD

A. Analysis in the variables P and q^2

In this work, we apply a method introduced in Ref. [7], which consists of using the variable $P = |\vec{P}|$, i.e., the modulus of the baryon-antibaryon relative three-momentum, in the baryon rest frame:

$$P = \sqrt{\left(\frac{q^2}{4M_B^2} - 1\right)q^2},\qquad(5)$$

where M_B is the baryon mass. In the near-threshold and the asymptotic regions such a variable behaves as

$$P \underset{q^2 \to \infty}{\simeq} \frac{q^2}{2M_B}, \quad P \underset{q^2 \to 4M_B^2}{\simeq} \sqrt{4M_B(\sqrt{q^2} - 2M_B)},\qquad(6)$$

(we also examine data for the $\Lambda\bar{\Sigma}^0$ transition TLFF, where the above equations are slightly modified due to the difference between the two hadron masses). As an example, for the neutron-antineutron case, P as a function of q^2 is shown in Fig. 1.

In the following we will compare TLFF data both in the same q^2 and in the same P conditions. As explicitly shown

in Eq. (5), P is a function of q^2 and of the baryon mass M_B. It follows that data at the same q^2 but for different channels, i.e., different baryon masses M_B, have different values of P. In each channel, by definition $P = 0$ when $q^2 = 4M_B^2$. For example, $P = 0$ in the $\Lambda\bar{\Lambda}$ channel corresponds to a rather large value of P in the nucleon channels, being $M_\Lambda > M_p, M_n$.

If some common phenomenon characterizes the $n\bar{n}$ and the $\Lambda\bar{\Lambda}$ final states produced through the annihilation reaction $e^+e^- \to B\bar{B}$, with $B = n$ or Λ, then this would manifest itself when comparing the outcome of the two channels at the same q^2, i.e., at different values of P. Only in the proton versus neutron case same q^2 and same P are equivalent concepts, because of their similar masses.

How should be interpreted a phenomenon occurring at the same P in two channels with baryons having different masses? Since same P implies different q^2, this phenomenon is not an effect of any communication between the channels, but it must be due to something that independently but similarly takes place in both channels at a given relative energy above threshold.

Another point distinguishes phenomena that appear as systematic in the same P or in the same q^2 view. Assume that the $e^+e^- \to B\bar{B}$ reaction proceeds through a perturbative QCD (PQCD) quark-gluon stage first, followed by the $B\bar{B}$ formation stage. The $B\bar{B}$ relative three-momentum $\vec{P}$ has no meaning in the initial stage. In fact, it cannot be defined until separated baryon and antibaryon emerge from the PQCD stage. So, whenever a phenomenon appears as systematic with respect to P but not to q^2, it has to be associated with interactions between the forming or formed baryons in a stage where their physical separation takes place.

B. Interpolation of reference for proton form factor

We will often use proton data as a reference, because of their unrivaled quality in terms of precision, range, continuity, and coherence between different measurements. However, in order not to overload the figures with data points, instead of the proton data, we may use the straight lines shown in Figs. 2 and 3 that indicate the quantities described in the following:

(i) The asymptotic horizontal linear fit of $(q^2)^2 F_p(q)$ in the q^2 range 5.5–13 GeV^2. We expect $(q^2)^2 F_p(q) \approx$ const. at large q^2, and this is the reason behind the above *fit*. Actually, two BABAR points with large error bars at q^2 between 20 and 25 GeV^2 (not shown in this figure) lie slightly below this line, suggesting that a really asymptotic trend has not been reached. For 5 GeV$^2 < q^2 < 13$ GeV^2, the above interpolation well averages the proton data and it is therefore later used as a reference in the figures showing baryon data versus q^2.

(ii) Two straight-line fits of F_p as a function of P in semilog plot. These are fits of the form e^{-aP}. The former fit is a basic background fit [as in Eq. (3)] interpolating the oscillating proton data in the near-threshold region, up to about $P = 3$ GeV. The latter well reproduces all the proton data in the region $P > 4$ GeV where oscillations are not visible anymore, and can be considered asymptotic, since it involves the largest q^2 available data.
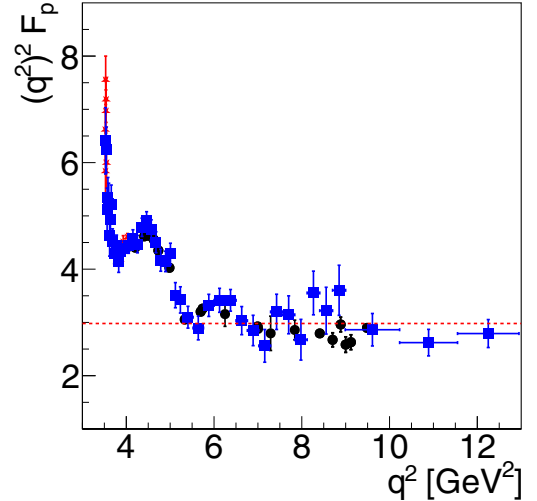

FIG. 2. Simple interpolation of proton data in a preasymptotic region. The data are F_p data from the BABAR Collaboration [5,6] (blue squares), the CMD-3 Collaboration [26,32] (red stars), and the BESIII Collaboration [12] (black circles). The dashed red horizontal line represents an interpolation of proton data for 5 GeV$^2 < q^2 <$ 13 GeV^2. This is not a precise fit but is useful for later comparison with baryon data presenting special features in that region.

III. RESULTS

A. Near-threshold $P \leqslant 2$ GeV range

The near-threshold behavior of the four lowest-mass species, two neutral (neutron and Λ) and two charged (proton and Σ^+) is shown in Fig. 4 as a function of $q = \sqrt{q^2}$. Although they show a similar qualitative behavior, it is difficult
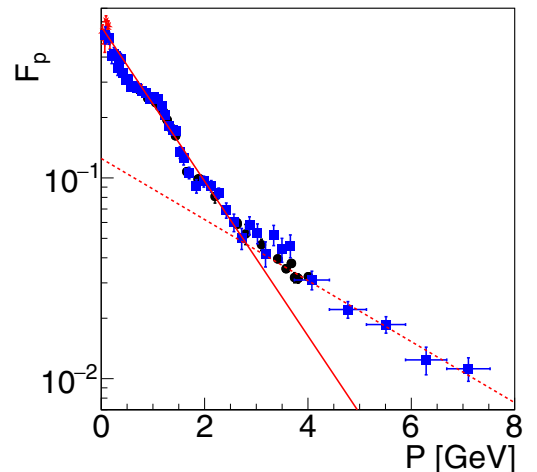

FIG. 3. Near-threshold and asymptotic interpolations of proton data versus P. The data are as in Fig. 2. The two straight lines show interpolations of the proton data for P smaller (larger) than 2.75 GeV, red solid line (red dashed line). Because of the semilog plots, these correspond to e^{-aP} shapes. Although we do not attribute any special meaning to these interpolations, they are used as a reference in later figures showing other baryon data, to compare them with proton data trends at small and large P.
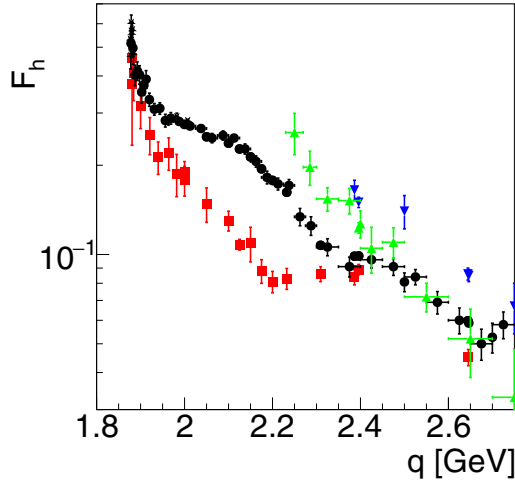
FIG. 4. TLFFs of proton (black circles), neutron (red squares), Λ (green triangles), and Σ^+ (blue down triangles) versus $q = \sqrt{q^2}$ in the region or relatively small q. Two charged and two neutral species characterized by small error bars have been selected for this figure. More species will be considered in the following, but presenting them altogether would make the picture difficult to read.

to find shared trends at a precise level, even if one substitutes proton and neutron with their background components, i.e., the average over local oscillations. The first difficulty is given by the different thresholds.

Neutral baryon TLFFs are shown in Fig. 5 as a function of P. We notice that in a semilog plot all the points organize themselves along straight lines with the same slope. The exception to this kind of neutral-baryon rule is that near-threshold Ξ^0 points, not reported in this figure, rise instead of falling.
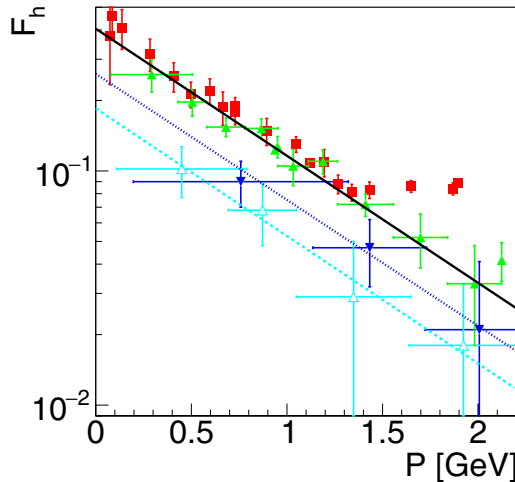

FIG. 5. TLFFs of neutron (red squares), Λ (green triangles), Σ^0 (blue down trianglens), and $\Lambda\bar{\Sigma}^0$ (open cyan triangles) transition TLFF (a neutral $\Lambda\bar{\Sigma}^0$ pair is produced), as functions of P in the near-threshold region. A solid black straight line is used to interpolate the neutron and Λ points, a dotted blue line with the same slope the Σ^0 points, and a dashed cyan line the $\Lambda\bar{\Sigma}^0$ points. Because of the semilog plot, these straight lines correspond to Ae^{-aP} exponential functions with different normalizations A but same slope a.
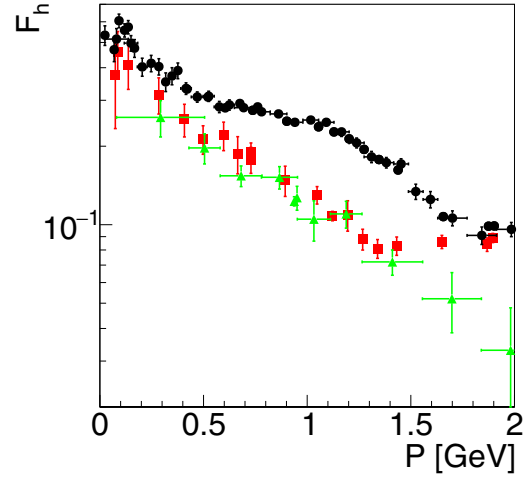

FIG. 6. Compared TLFF of neutron (red squares), Λ (green triangles), and proton (black circles) versus P. One may notice the separation of proton points from neutron and Λ just above threshold. Neutron and Λ points follow the same trend up to $P = 1.5$ GeV. Above this value, neutron data converge to the proton data.

Neutron data practically coincide to those of the Λ up to $P = 1.2$ GeV, then they change slope, anticipating what the other TLFFs do at larger P. A straight line allows us to appreciate the slope. Two more straight lines parallel to the neutron and Λ line are shown. One is compatible with the Σ^0 points, the other one with the data of the $\Lambda\bar{\Sigma}^0$ transition TLFF. Neutron, Λ, Σ^0 and $\Lambda\bar{\Sigma}^0$ TLFFs have a very similar near-threshold behavior, which, instead, is quite different from that of the other baryons. In Fig. 6 the neutron and Λ TLFFs are compared to the proton one in the same range. A plain observation shows two facts:

(i) Near the threshold, all data coincide, but just above a separation takes place with a softer average slope for the proton.

(ii) At $P = 1.2$ GeV the neutron values move away from the Λ ones and reach the proton data.

This relative proton-neutron behavior is the ground for the joint oscillation fit with a phase difference proposed in Ref. [13]. Any phase difference requires the two to immediately separate and periodically rejoin. Whatever the interpretation, the initial average slope of the proton F_p is different from the common slope of neutron and Λ, that is the same as for Σ^0 and $\Lambda\bar{\Sigma}^0$.

The charged FFs presently available are compared with the proton one, together with the Ξ^0 isospin partner of Ξ^- to check for correlations in the variable P in Fig. 7 and in the variable q^2 in Fig. 8. These data, plotted as a function of P, show that the behavior of the charged baryons and of Ξ^0 is different with respect to the considered neutral ones but presents common peculiarities. In particular a rich peak/shoulder structure is present.

Plotting for the same baryons $(q^2)^2 F_h(q^2)$ with respect to q^2 shows a good correlation between the oscillations of the baryons and the second, the third, and fourth oscillation that could actually consist of two separate peaks. Indeed, although
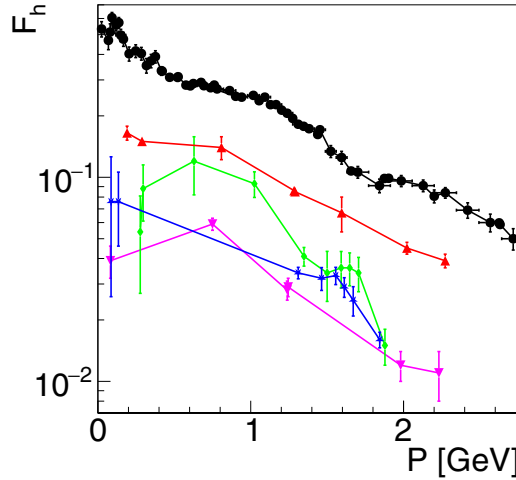
FIG. 7. F_h versus P or Σ^+ (red triangles), Σ^- (magenta down triangles), Ξ^- (blue stars), and Ξ^0 (green diamonds), together with proton data (black circles). Since points of different sets overlap, we have used segments to join the points of the same set (in the proton case, we have three sets of data, see Fig. 2). The most remarkable feature here is the presence of a correlated peak/shoulder for Σ^+ and Σ^-, and the presence of two peaks in the case of Ξ^0, one correlated with Ξ^- and one with Σ^- and Σ^+. These data have a correspondence with the peak-rich structure of the proton (black solid circles).

the proton points appear as randomly oscillating, their oscillations are well correlated with the oscillations of all the other baryons.
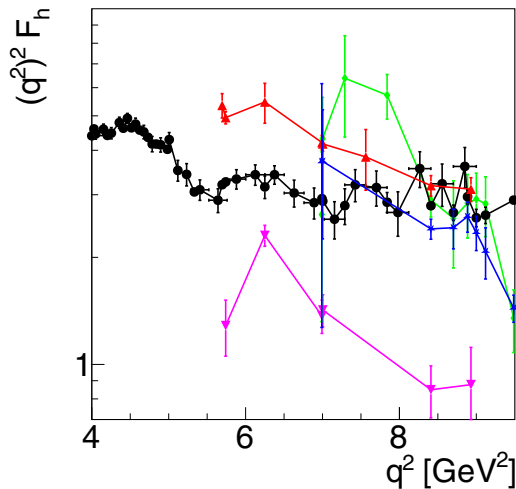

FIG. 8. $(q^2)^2 F_h$ for Σ^+ (red triangles), Σ^- (magenta down triangles), Ξ^- (blue stars), and Ξ^0 (green diamonds), together with proton data (black circles). Since points of different sets overlap, lines connect the sequence of points of the same set (in the proton case, three sets of data are drawn, see Fig. 2). The strong correlation between the peaks of different data is evident and suggests that the fourth proton maximum is not a statistical fluctuation, but consists of at least one and perhaps a pair of maxima, correlated with a peak-dip-peak sequence part of which has a correspondence, for example, in the Ξ^0 data.

In the P plot we find a coincidence between peak/shoulders of Ξ^0 and $\Sigma^\pm$, but a similar coincidence occurs between different maxima in the case of the q^2 plot. This looks like a random effect due to the mass difference between the two channels coinciding with the shift between different maxima in the same channel. Summarizing what we may conclude from these two figures:

(i) Maxima do evidently exist in the charged baryon data and their correlation shows that they are not due to data fluctuations over underestimated statistical errors. In the case of Ξ^0 at least two maxima are well visible and both coincide with maxima of other baryons.

(ii) The fourth proton oscillation maximum may not be a random fluctuation of the data in a region where error bars have the same magnitude as the oscillation amplitude.

(iii) The well-correlated oscillations of Σ^+ and Σ^- effective TLFFs are less predictable than one could expect, since these two baryons are not antiparticles of each other and have a slightly different mass. Their third isospin partner Σ^0 behaves in a different way, as shown in other figures.

B. Comparison among strangeness 0 and 1, neutral versus proton, in a broader range

Proton data cover a much larger range than any other. As shown in Refs. [7,8] where a 5–10 % oscillating modulation is subtracted, the leading background follows a regular trend, described by a q^2 tripole. However, the TLFFs of neutral baryons shown here present a steeper near-threshold fall.

This argument does not change comparing data at the same q^2. Measured values of the effective TLFF of all baryons near their thresholds are larger than the proton one, but they decrease within shorter energy intervals, i.e., they have a steeper decreasing behavior.

On the other side the arguments leading to the $(1/q^2)^2$ asymptotic behavior with logarithmic corrections for the leading F_1 helicity-conserving component of the TLFFs, have not met serious challenges up to now. So we face three possibilities.

(i) Neutral baryon TLFFs follow an asymptotic behavior as $\simeq A/(q^2)^2$ while $F_p \simeq B/(q^2)^2$ with $A \ll B$.

(ii) In the region separating near-threshold and asymptotic q^2, one strong oscillation at least is present, that allows the neutral FFs to rise up to proton-like values at large q^2.

(iii) Because of a suppression of the leading helicity-conserving F_1 term, the $1/(q^2)^2$ trend is not reached in the investigated q^2 region.

The quark counting rule predicting the $\simeq A/(q^2)^2$ asymptotic behavior does not constrain the magnitude of A. On the other side, for A to be very different from case to case, one should imagine either a suppression mechanism, acting in some cases but not in general, or a very different formation path for different baryon-antibaryon pairs. At large q^2, SU(3)
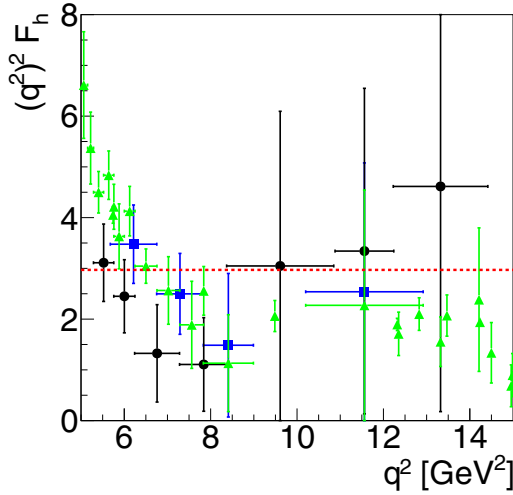
FIG. 9. $(q^2)^2 F_h$ as a function of q^2 for Λ (green filled triangles), Σ^0 (blue squares), and transition $\Lambda\bar{\Sigma}^0$ (black circles) data. The horizontal red dashed line is the proton preasymptotic fit of Fig. 2. A coherent minimum-maximum sequence is visible in the cumulative set of strange neutral baryons, that does not show simple correlations with the structures in Fig. 8. Roughly, the minimum here is not far from a maximum in Fig. 8.

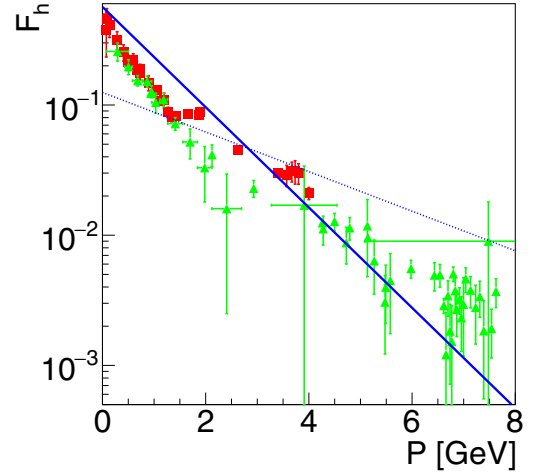FIG. 10. Λ and neutron TLFFs as a function of P. The straight lines are the proton TLFF interpolations of Fig. 3 at small-P (solid blue line) and large-P (dotted blue line). At small P neutron and Λ data coincide and have a steeper fall than proton data. At $P > 2$ GeV, neutron data reach the proton values. Above $P = 4$ GeV no neutron data are available, while Λ data are in the average steeper than proton data, and show hints of minima at 5.5, 6.7, 7, 7.5 GeV. In this region only proton and Λ data are available.

symmetry should be restored, implying differences such as $\sqrt{3}/2$ or so between the different baryon FFs. These considerations would favor case (ii) in the previous list, what will be checked in future data.

For the effective FFs of the charged strange baryons and of the neutral Ξ^0, only the near-threshold data shown in the previous figures exist, so they are not considered in this section. For the neutron and the strange baryons effective TLFFs the data span a medium kinematical range, meaning the region of P up to 10 GeV. Their behavior is, however, not homogeneous, so they are discussed separately, using proton data as a reference. Specifically for Λ, recent measurements are available for q^2 values larger than those of the other neutral baryons.

Figure 9 shows a clean example of a case (ii). In the region $\sqrt{q^2} = 5 - 15$ GeV, the quantity $(q^2)^2 F_h(q^2)$ is almost constant for the proton; it is represented by a thick horizontal dashed line. On the contrary, for the TLFF of Λ and Σ^0, and the $\Lambda\bar{\Sigma}^0$ transition TLFF an initial steep decrease is followed by a rise that leads the data at the proton values again.

C. Effective form factors of the Λ compared to the nucleons

Figure 10 shows the data of the Λ and the neutron effective TLFFs, together with the straight lines that interpolate the behavior of proton data at P below and above 4 GeV reported in Fig. 3. Both neutron and Λ data, after the initial steep decrease, show a rise as a tendency to reach the proton values. Such a tendency is fully realized in the case of the neutron at $P \approx 2$ GeV and $P \approx 4$ GeV. What happens precisely in between is not clear yet as there are no data at larger energies.

For $P > 5$ GeV, neutron data are not present anymore and only F_Λ may be compared with F_p. The surprising recent BE-

SIII Λ data at large P follow the extrapolation of the small-P proton data. Visibly, the F_Λ values at large P spread over a region where F_Λ is smaller than F_p by a factor that ranges from 0.1 up to 0.6. The data also seem to suggest that F_Λ may present some deep minima in this region, however, the data points are dense and it is difficult to distinguish physical from statistical fluctuations.

IV. CONCLUSIONS

The existing data on baryon TLFFs were collected and compared in the attempt of finding common features and highlight the kinematical region and the reactions where future data are highly desirable. The comparison of the data in terms of two kinematical variables P and q^2, allows to visualize possible correlations and make conjectures about their origin.

The presence of three oscillations in proton TLFF data is a well-known fact by now, but a visible fourth oscillation maximum is still ambiguous because of errors. The presence at the same q^2 of oscillation maxima of other baryon TLFFs (Fig. 8) supports the physical reality of this maximum in the proton data.

The F_Λ at high q^2 shows possible structures, with up to four minima that could be very deep, or just be due to local error dilatation. Further precise data in this region may clarify these structures, as well as the asymptotic behavior, clearly steeper than the proton one.

Neutron and Λ data show several similarities, but continuous neutron data stop at $\sqrt{q^2} = 2.4$ GeV, with a few more scattered points at larger q^2. These may be compatible either with proton-like regular oscillations, or with Λ-like behavior. Continuous neutron data over 2.4 GeV are needed to clarify

what could be a complex network of correlations between neutron, proton and Λ.

Baryon data near their respective thresholds can be divided into two groups with very different behavior. This difference is so marked that more precise data could not overthrow it. The case of the strangeness-1 neutral baryons, including the transition $\Lambda\bar{\Sigma}^0$ TLFF, is especially interesting since they seem to present the same marked down-up-down change of slope at $q^2 \approx 10$ GeV^2, possibly overlapping. The neutron shows a very similar feature at smaller q^2. So, more precise data in this region could show interesting and unpredicted phenomena.

An important limitation of the present knowledge of F_h is an almost complete lack of information on the phases of G_E and G_M. Experiments with measures of the final polarizations will give further insight to this question. In this respect, limited results for a very small number of definite values of q^2 on the phase of G_E/G_M for the Λ hyperon have been extracted by the BaBAR Collaboration [18] and, more recently, by the BESIII experiment [33]. These data have been used to further constrain the analytical properties of FFs in Ref. [34].

The present analysis is not based on models and focusses on general features that can be extracted from the data and from kinematical considerations.

Summarizing, although the proton data oscillation is already something that escapes obvious interpretations, the landscape of the baryon data could be far richer, and new precise measurements will surely show surprising features.

Further information from TLFFs is contained in the time-reversed reactions induced by antiproton and antineutron beams. In the future, the PANDA experiment at FAIR is expected to run an important program of FF measurements [35], by considering the processes $p\bar{p} \to e^+e^-$, $\mu^+\mu^-$ [36,37]. A discussion of the presented data, in connection with possible formation mechanisms, will be presented in a forthcoming paper.

[1] S. Pacetti, R. Baldini Ferroli, and E. Tomasi-Gustafsson, Phys. Rep. **550**, 1 (2015).

[2] A. Denig and G. Salme, Prog. Part. Nucl. Phys. **68**, 113 (2013).

[3] A. Antonelli *et al.*, Phys. Lett. B **313**, 283 (1993).

[4] V. N. Baier, E. A. Kuraev, V. S. Fadin, and V. A. Khoze, Phys. Rep. **78**, 293 (1981).

[5] J. Lees *et al.* (BaBar Collaboration), Phys. Rev. D **87**, 092005 (2013).

[6] J. Lees *et al.* (BaBar Collaboration), Phys. Rev. D **88**, 072009 (2013).

[7] A. Bianconi and E. Tomasi-Gustafsson, Phys. Rev. Lett. **114**, 232301 (2015).

[8] A. Bianconi and E. Tomasi-Gustafsson, Phys. Rev. C **95**, 015204 (2017).

[9] A. Bianconi and E. Tomasi-Gustafsson, Phys. Rev. C **98**, 055204 (2018).

[10] M. Ablikim *et al.* (BESIII Collaboration), Phys. Rev. D **91**, 112004 (2015).

[11] M. Ablikim *et al.* (BESIII Collaboration), Phys. Lett. B **817**, 136328 (2021).

[12] M. Ablikim *et al.* (BESIII Collaboration), Phys. Rev. Lett. **124**, 042001 (2020).

[13] M. Ablikim *et al.* (BESIII Collaboration), Nature Phys. **17**, 1200 (2021).

[14] M. Ablikim *et al.* (BESIII Collaboration), Phys. Rev. D **97**, 032013 (2018).

[15] M. Ablikim *et al.* (BESIII Collaboration), Phys. Rev. D **104**, L091104 (2021).

[16] M. Ablikim *et al.* (BESIII Collaboration), Phys. Lett. B **814**, 136110 (2021).

[17] M. Ablikim *et al.* (BESIII Collaboration), Phys. Lett. B **831**, 137187 (2022).

[18] B. Aubert *et al.* (BaBar Collaboration), Phys. Rev. D **76**, 092006 (2007).

[19] S. Dobbs, K. K. Seth, A. Tomaradze, T. Xiao, and G. Bonvicini, Phys. Rev. D **96**, 092004 (2017).

[20] M. Ablikim *et al.* (BESIII Collaboration), Phys. Rev. D **103**, 012005 (2021).

[21] M. Ablikim *et al.* (BESIII Collaboration), Phys. Lett. B **820**, 136557 (2021).

[22] V. Matveev, R. Muradyan, and A. Tavkhelidze, Teor. Mat. Fiz. **15**, 332 (1973).

[23] S. J. Brodsky and G. R. Farrar, Phys. Rev. Lett. **31**, 1153 (1973).

[24] I. T. Lorenz, H. W. Hammer, and Ulf-G. Meißner, Phys. Rev. D **92**, 034018 (2015).

[25] J. P. B. C. de Melo, T. Frederico, E. Pace, and G. Salme, Phys. Lett. B **581**, 75 (2004).

[26] R. R. Akhmetshin *et al.* (CMD-3 Collaboration), Phys. Lett. **B794**, 64 (2019).

[27] E. Tomasi-Gustafsson, A. Bianconi, and S. Pacetti, Phys. Rev. C **103**, 035203 (2021).

[28] R. Baldini, S. Pacetti, A. Zallo, and A. Zichichi, Eur. Phys. J. A **39**, 315 (2009).

[29] X. Cao, J.-P. Dai, and H. Lenske, Phys. Rev. D **105**, L071503 (2022).

[30] Y.-H. Lin, H.-W. Hammer, and Ulf-G. Meißner, Phys. Rev. Lett. **128**, 052002 (2022).

[31] A.-X. Dai, Z.-Y. Li, L. Chang, and J.-J. Xie, arXiv:2112.06264.

[32] R. Akhmetshin *et al.* (CMD-3 Collaboration), Phys. Lett. B **759**, 634 (2016).

[33] M. Ablikim *et al.* (BESIII Collaboration), Phys. Rev. Lett. **123**, 122003 (2019).

[34] A. Mangoni, S. Pacetti, and E. Tomasi-Gustafsson, Phys. Rev. D **104**, 116016 (2021).

[35] B. Singh *et al.* (PANDA Collaboration), Eur. Phys. J. A **52**, 325 (2016).

[36] G. Barucca *et al.* (PANDA Collaboration), Eur. Phys. J. A **57**, 30 (2021).

[37] A. Dbeyssi, E. Tomasi-Gustafsson, G. I. Gakh, and M. Konchatnyi, Nucl. Phys. A **894**, 20 (2012).